Computer-Aided Intra-Operatory Positioning of an MRgHIFU Applicator Dedicated to Abdominal Thermal Therapy Using Particle Swarm Optimization

Yacine M'Rad, Caecilia Charbonnier ⓘ, Marcelo Elias de Oliveira ⓘ, Pauline Coralie Guillemin,
Lindsey Alexandra Crowe, Thibaud Kössler, Pierre-Alexandre Poletti, Sana Boudabbous ⓘ,
Alexis Ricoeur, Rares Salomir, and Orane Lorton ⓘ

Abstract—Purpose: Transducer positioning for liver ablation by magnetic resonance-guided high-intensity focused ultrasound (MRgHIFU) is challenging due to the presence of air-filled organs or bones on the beam path. This paper presents a software tool developed to optimize the positioning of a HIFU transducer dedicated to abdominal thermal therapy, to maximize the treatment's efficiency while minimizing the near-field risk. Methods: A software tool was developed to determine the theoretical optimal position (TOP) of the transducer based on the minimization of a cost function using the particle swarm optimization (PSO). After an initialization phase and a manual segmentation of the abdomen of 5 pigs, the program randomly generates particles with 2 degrees of freedom and iteratively minimizes the cost function of the particles considering 3 parameters weighted according to their criticality. New particles are generated around the best position obtained at the previous step and the process is repeated until the optimal position of the transducer is reached. MR imaging data from *in vivo* HIFU ablation in pig livers was used for ground truth comparison between the TOP and the experimental position (EP). Results: As compared to the manual EP, the rotation difference with the TOP was on average $-3.1 \pm 7.1°$ and the distance difference was on average -7.1 ± 5.4 mm. The computational time to suggest the TOP was 20s. The software tool is modulable and demonstrated consistency and robustness when repeating the calculation and changing the initial position of the transducer.

Index Terms—Computer-aided positioning, HIFU transducer, near-field safety, particle swarm optimization (PSO), thermal therapy.

Impact Statement— The software tool using the PSO algorithm suggests the optimal positioning of the transducer for abdominal MRgHIFU ablations. The software tool is consistent, accurate and user friendly.

I. INTRODUCTION

HIGH-INTENSITY focused ultrasound (HIFU) is a non-invasive ablation technique for the treatment of solid tumors. Magnetic resonance imaging (MRI) is an advanced tool used for therapeutic ultrasound guidance providing near real-time temperature monitoring and high-resolution (HR) 3D anatomical images [1], [2], [3], [4]. Magnetic resonance guided HIFU ablation (MRgHIFU) in the liver is very promising for the treatment of primary cancer such as hepatocellular carcinoma, as well as secondary cancer, which is the most prevalent cancer in the liver and mainly arises from gastro-intestinal cancer [5], [6]. Liver ablation could be particularly useful for the treatment of metastatic colorectal cancers, as one third of the patients with colorectal cancer will experience hepatic metastatic disease [7] with more than 80% of the metastatic colorectal cancers are surgically ineligible [8], [9]. A tumor is considered as treatable by HIFU if clearly visible under MR or US, and CT, and if technically and safely reachable by HIFU, considering the vicinity of adjacent structures (main bile ducts, gallbladder, bowel, stomach), as well as the specific transducer's geometry. A large meta-analysis found the average tumor size treated by HIFU to be 5.1 cm [10], while the targetable regions are in liver segments II to VIII. However, HIFU lesioning in the liver is very challenging due to the presence of critical surrounding organs,

typically air-filled structures and bones. Ultrasound propagation through tissues with significant impedance change is subject to undesirable effects at interfaces, including absorption, reflections, standing waves, and focal point shift. The higher energy absorption rate of the bone, approximately a factor of 12 compared to the soft tissues [11] may induce substantial heating in the near field (e.g rib cage) and may even propagate into skin burns or infiltrating thermal lesions [12], [13], [14]. Breathing motion has been addressed by numerous reports, for instance using two-dimensional ultrasound imaging [15], [16], [17] or a one-dimensional MR navigator [18]. Accordingly, motion encoding was used to correct the HIFU ablation for liver displacement in real-time, either by modulating the emitted power to uniformly increase the temperature along a linear pattern ("self-scan"), or by electronically steering the focus to track-and-lock on the anatomic target.

In 2014, Anzidei et al. [19] reported a successful non-invasive treatment of hepatocellular carcinoma by MRgHIFU in one patient, but they highlighted the limitations induced by the presence of the rib cage. Several solutions have been proposed to manage the rib cage issue, such as partial rib resection before the HIFU intervention [20], [21]. This surgical solution is in flagrant contradiction with the minimally-invasive nature of the intervention but offers a solution when no other treatments are practicable. Another approach was the development of software method such as de-activation of chosen elements based on shadowing [22] or algorithms that consider the diffraction and interferences to maximize the energy deposited at the focus versus the ribs [23], [24]. Element selection demonstrated benefits for reduction of side lobes and bone heating, as well as better focusing despite reasonable loss of energy deposition at the focus. Salomir et al. [25] inserted anechoic reflective strips in front of the ribs. Ramaekers et al. [26] designed Voronoi-tessellated transducers based on Fermat's spiral. As a matter of principle, avoiding the need for rib protection would facilitate the workflow and also eliminate the risk of procedural errors.

Auboiroux et al. [27] divided the full array of transducers into multiple sub-arrays of different resonance frequencies. The passive spectral multiplexing combined with the reorientation of these individual emitters enabled the augmentation of the steering range by 80% along one preferentially chosen axis.

Very recently, Lorton et al. [11], [28] presented a new concept of transcostal HIFU transducer able to thermally ablate in vivo deep-seated targets of pig livers. The feasibility and targeting accuracy of tumor ablation located in regions considered as challenging to resect was demonstrated in 6 pig livers. The study reported 5 thermal ablations with a 2.4 ± 2.0 mm targeting accuracy. The measured temperature on the target reached 58–86 °C spatial average, with a safe ratio between the temperature elevation at the target versus the ribs, in average 7.3. No specific means of protection were needed for the ribs. The weakness of that study was the manual adjustment of the transducer position in front of the abdominal wall, with successive visual check points and re-acquisition of 3D MR datasets. Besides being time consuming, this approach does not guarantee the optimal position of the applicator with respect to the near field safety. To summarize the problem, the main issue in HIFU liver ablation

is to find the best entry window which minimizes the energy depletion and heating on the beam pathway, while maximizing the amount of energy effectively delivered at the target.

Some theoretical considerations can be inferred from the skull issue which has been already investigated in the context of the HIFU therapy in brain. A method based on the minimization of the average reflection coefficient (ARC) was developed to find the optimal transducer position of a single-element transducer [29]. Another way is to use the inverse problem to calculate all the possible positions for the transducer by computing the phase distribution from a target point [30]. This technique leads to the best transducer position but requires high computational power. In 2022, Park et al. [31] reported time-reversal simulations using the target as ultrasound source. However, the prescribed lesion shape may significantly impact the optimal position, and the simulation accuracy may vary when using other frequencies, leading to spreading of results. Overall, transskull HIFU sonication has the advantage of a near hemispherical entry window, while transcostal HIFU sonication only exploits a limited solid angle.

In this paper, we present a novel software tool developed to automatically optimize the transducer positioning for abdominal HIFU, first of the kind in a target organ other than the brain. Based on the segmentation of 3D MR images, it determines the theoretical optimal positioning (TOP) of the device using the particle swarm optimization (PSO) [32]. The software was used on retrospective data of MRgHIFU ablations of in vivo pig livers to evaluate the applicability and relevance.

II. MATERIALS AND METHODS

A. Design of the Transducer

The device is a phased-array transducer dedicated to transcostal liver ablation [11], [28] (Imasonic, Voray-sur-l'Ognon, France) working at 650 kHz. The 256-element transducer is populated with elements widely distributed on 5 concentric segments of spheres of different radii (100, 111 and 124 mm) to increase the contact surface with the skin while guaranteeing a natural focal point at 10 cm-depth (Fig. 1(a)), see Supplementary Material for more details. Eight sharp features have been defined on the computer-aided design (CAD) (Fig. 1(a)) enabling further registration on the 3D MR images. The lesion size in this paper is limited to fixed focus ablation, on the order of 1cc. Larger lesion would require electronic beam forming of foci pattern, which could affect the solution of the optimal positioning. The eligible target location is restricted to the volume of the liver reachable by the acoustic focus, meaning the entire liver minus a 2 cm safety margin in 3D space.

B. Software Design

The software was designed to optimize the transducer's position relative to the patient anatomy and target location, by minimizing a cost function using the PSO algorithm. HR 3D MR images (see Supplementary Material for sequence details) of 5 pigs which received an MRgHIFU liver ablation were retrospectively used and imported into free open-source software 3D
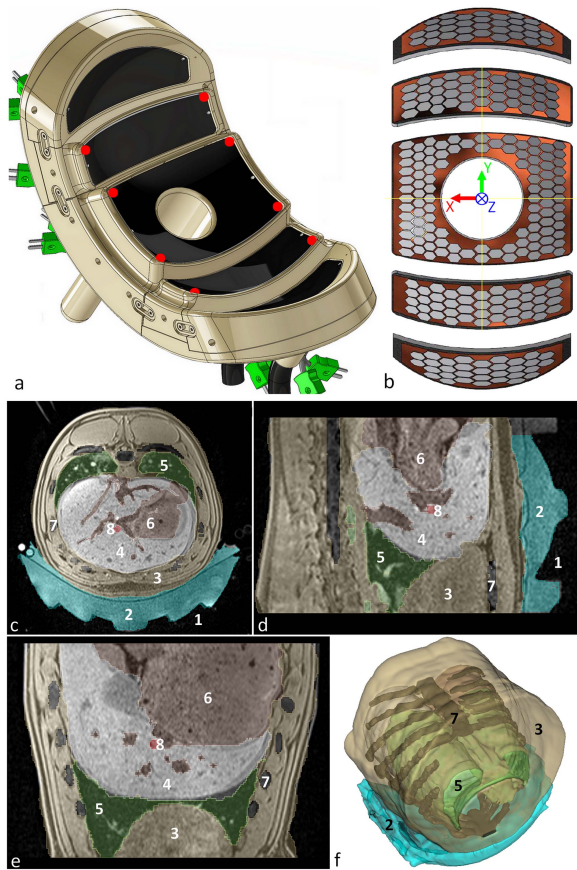
Fig. 1. (a) 3D computer-aided design of the transducer showing the five concentric parts of sphere. The red dots correspond to the eight sharp features. (b) Rear view of the 256 individual emitters populating the phased-array transducer. Segmentation of the different tissues and structures on high resolution 3D MR images using 3D slicer on the (c) axial, (d) sagittal and (e) coronal planes. (f) 3D representation of the segmentation. 1. HIFU transducer, 2. Acoustic coupling, 3. Soft tissues, 4. Liver, 5. Lungs, 6. Vessels, 7. Bones, 8. HIFU lesion.

slicer [33] for manual segmentation of the different structures (see Fig. 1(a)–(d)). The CAD of the transducer containing the centre of mass of each individual acoustic element was also imported into the optimization software for the calculation of the cost function (Fig. 2(b) and (c)). After setting initial parameters (detailed in a dedicated section below), the software minimized the specific cost function using the PSO and displayed the coordinates of the TOP along the chosen degrees of freedom (DoF), as well as the 3D representation.

Various DoF can be considered for the mechanical displacement of the HIFU applicator. Here, we identified the most relevant two DoF as 1) the radial distance from the skin to the applicator, and 2) the applicator rotation around the cranio-caudal axis.

The retrospective in vivo MR data and setup were finally used to compare the experimental position (EP) and the TOP and to assess the relevance of this tool.

C. Particle Swarm Optimization (PSO)

The PSO algorithm [32] consists in generating a swarm of potential solutions, called particles, able to move in the coordinate frame defined by the DoF, also called the search space.
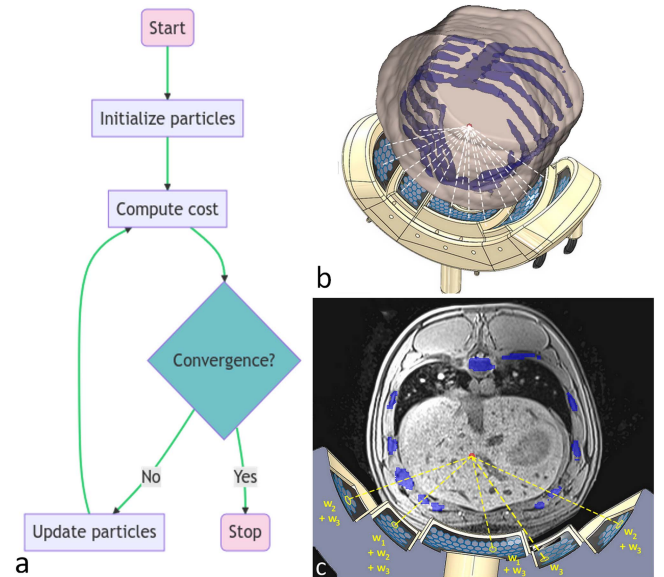

Fig. 2. (a) Chart of the PSO algorithm used to find the TOP. (b) 3D volume of the segmentation of the body and of the bones lying on the CAD of the transducer. The cone-beam targeting is represented by the white dotted lines. (c) Augmented reality of the transducer on a T1-weighted MR image of the pig in axial plane merged with the segmented bones (blue ROIs). The yellow dotted lines indicate the path from a transducer element to the target and the weight involved in the calculation of the cost function.

The particles are characterized by a position and velocity and iteratively move according to their own best-known position, and the entire swarm's best-known position, to converge to an optimized solution. In our specific case, the TOP is the best achievable, patient-specific, position of the transducer for liver ablation with minimized risks of bone heating. Fig. 2(a) shows the PSO applicable to our problematic and the different steps of the PSO algorithm are described in Supplementary Material.

For each acoustic element ($i = 1{:}N$, here N = 256), a straight ray is defined from the center of the element to the target, to check which tissues are on the path (Fig. 2(b) and (c)). The parameters of the cost function were chosen considering the most critical adjustments to find the TOP. As a component inside the body is inconceivable, the first term "*elementIsInsideSurface*" was designed to significantly increase the cost function aiming to exclude this case. A bone in the ultrasound path is not desired but not limiting the ablation, so the more elements in front of the ribs, the higher the cost function via the second term "*isBoneInUltrasoundPath*". The third term "*distanceToSurface*" is of interest for a convergent beam, because the closer the transducer to the skin, the lower the local acoustic intensity on the ribs, and, therefore, the lower the risk of heating. Overall, the lower the cost function, the more appropriate the position of transducer. The cost function to minimize is defined as follow:

$$cost = \sum (w1.elementIsInsideSurface(i)$$
$$+ w_2.isBoneInUltrasoundPath(i)$$
$$+ w_3.distanceToSurface(i)) \qquad (1)$$

Each term was weighted by a preset value (w_1, w_2, w_3) depending on their criticality, as defined below. A schematic
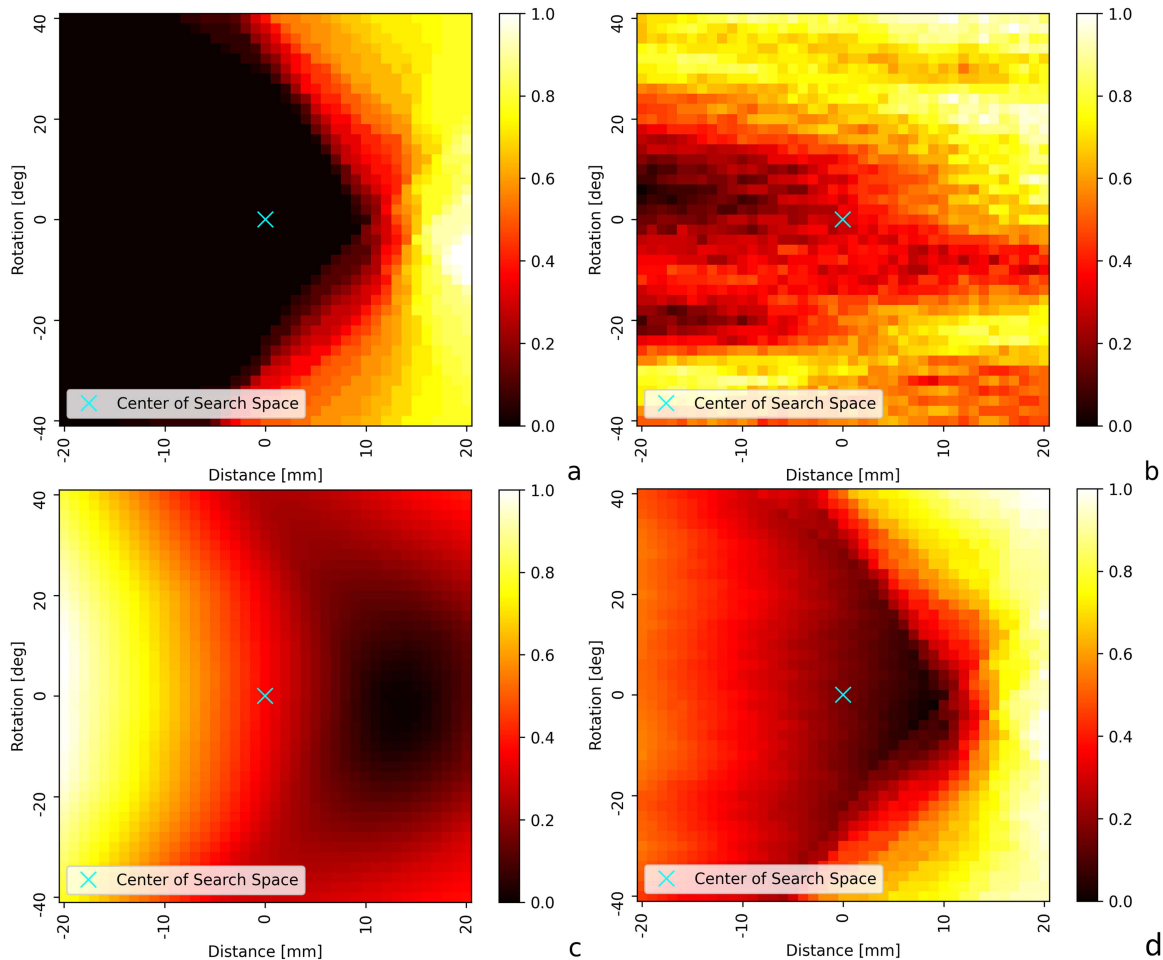
Fig. 3. Heatmaps of each cost component and their balanced combination of weights $(\frac{1}{3}, \frac{1}{3}, \frac{1}{3})$, as a function of two independent DoF, here the distance to skin and the rotation angle around the cranio-caudal axis. Darker pixels indicate lower cost, hence better coordinate of the HIFU applicator. (a) Cost heatmap representing the influence of the 'Inside Body' component. (b) Cost heatmap detailing the effect of the 'Bones in Path' component. (c) Cost heatmap showcasing the impact of the 'Distance from Element to Skin' component. (d) Heatmap displaying the combined costs with equal contributions from each component.

example of the weights involved in the calculation of the cost function is available in Fig. 2(c). As a result, the software provides the relative transform between the current segmented transducer's position and the optimally computed placement.

D. Weighting Factors of the Cost Function

The focus on two DoF to optimize enables us to represent the cost function as a 2D heatmap for analysis purpose, providing a visual understanding of each component's contribution. In the ensuing analysis, we offer a visual depiction of the unique and combined effects of various cost function components within our PSO algorithm. Each part of Fig. 3(a)–(d) represents a different cost function component for a single pig, illustrating its distinct contribution to the overall cost calculation. Fig. 3(d) integrates all three components, demonstrating the collective effect when all weights are uniformly set to 1/3.

The weighting of each cost component is certainly open to discussion (Fig. 4(a)–(d)). We opted for the combination $w_1 = 3/6$, $w_2 = 2/6$, $w_3 = 1/6$ based on the prioritization of the

cost function components. The highest importance was given to "Inside Body", ensuring the transducer doesn't enter the body, followed by the "Bones in Path" and the "Distance to surface" components, respectively.

E. Initial Parameters

The inertia, both cognitive and social parameters were fixed to 0.5 by providing a balance between exploration and exploitation behavior in the search space. To reduce the complexity of the problem, the applicator was considered symmetrically aligned on the anatomic axial plan crossing the target. The transducer's main z-axis, (Fig. 1(b)), contained in the anatomic axial plane is crossing the target with pinpoint accuracy. The TOP is defined in a coordinate system that includes rotation around the cranio-caudal axis (trigonometric degrees) and radial distance to the target (mm). The transducer is positioned outside the body at a default distance of 10 cm from the target, which corresponds to its natural focal length. Particles are initialized within a search
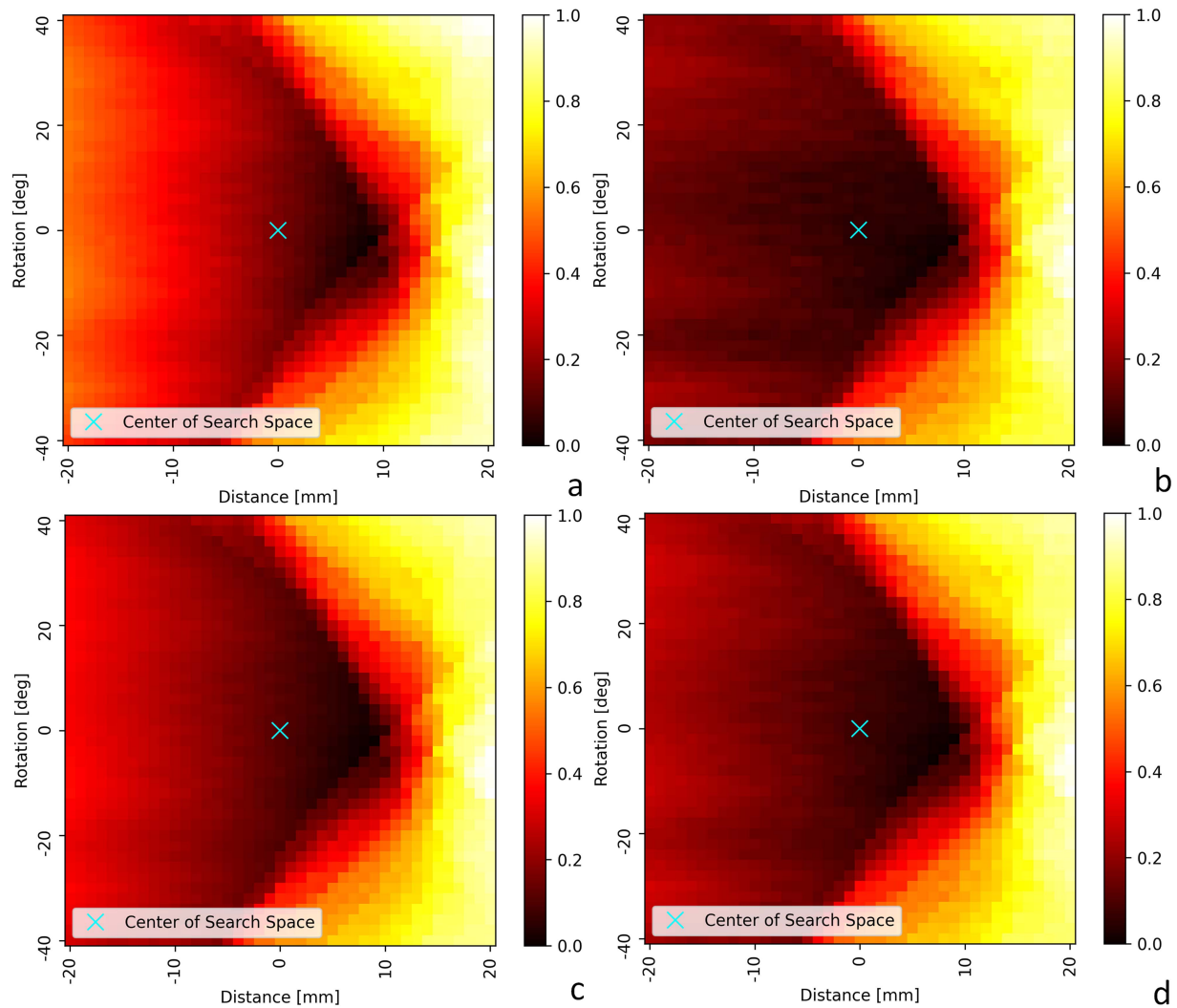
Fig. 4. Display of the global cost function using various component weights showing the significance of the weighting. w1 represents the "Inside Body" component, w2 represents the "Bones in Path" component, and w3 represents the "Distance from Element to Skin" component. (a) Heatmap with weight configuration $w_1 = 2/5$, $w_2 = 1/5$, $w_3 = 2/5$. (b) Heatmap with weight configuration $w_1 = 3/6$, $w_2 = 2/6$, $w_3 = 1/6$. (c) Heatmap with weight configuration $w_1 = 3/6$, $w_2 = 1/6$, $w_3 = 2/6$. (d) Heatmap with weight configuration $w_1 = 2/4$, $w_2 = 1/4$, $w_3 = 1/4$.

area around this initial transducer position, within an acceptable range in terms of physical implementation defined as $[-40, 40]°$

The range for varying the distance to the target was set to $[-20, 20]$ mm as this corresponds to the electronic beam capacities of the transducer along the z-axis. These ranges provide a comprehensive yet focused search space for the PSO algorithm to explore and identify the optimal transducer placement. The number of particles and iterations is a tradeoff between finding the near overall optimal position and the computation time. We empirically determined them to be 20, as the algorithm commonly reached a plateau by the 10th iteration. Increasing the number of particles would lead to longer computation time. Further iterations beyond this point yielded only marginal improvements to the cost function. To mitigate the risk of converging to local minima due to the non-continuous nature of the cost function, the algorithm was repeated three times with new random particle placement.

F. Evaluation

The relevancy of the software was validated by comparing the TOP to the EP of the transducer during an *in vivo* MRgHIFU ablation of 5 pig livers as approved by the ethical approval from the local animal research committee. A radiofrequency marker mimicking a target metastasis was created in a location considered difficult to resect at a 4–6 cm depth from the anterior liver capsule. The EP was considered as the ground truth as the actual MRgHIFU interventions in 5 pig livers conducted to thermal ablation ranging 58–86 °C at the expected target location. The thermal ablations were confirmed by gross pathology 7 days post-intervention. During post mortem examination, no skin lesions were detected on the thoracic and abdominal regions. A few millimeter-sized rib thermal lesions of grade 1 (6/6) were assigned, without any evidence found during post-mortem examination [11]. Here, the target of the EP was the center of mass of the effective thermal ablation. More details about the
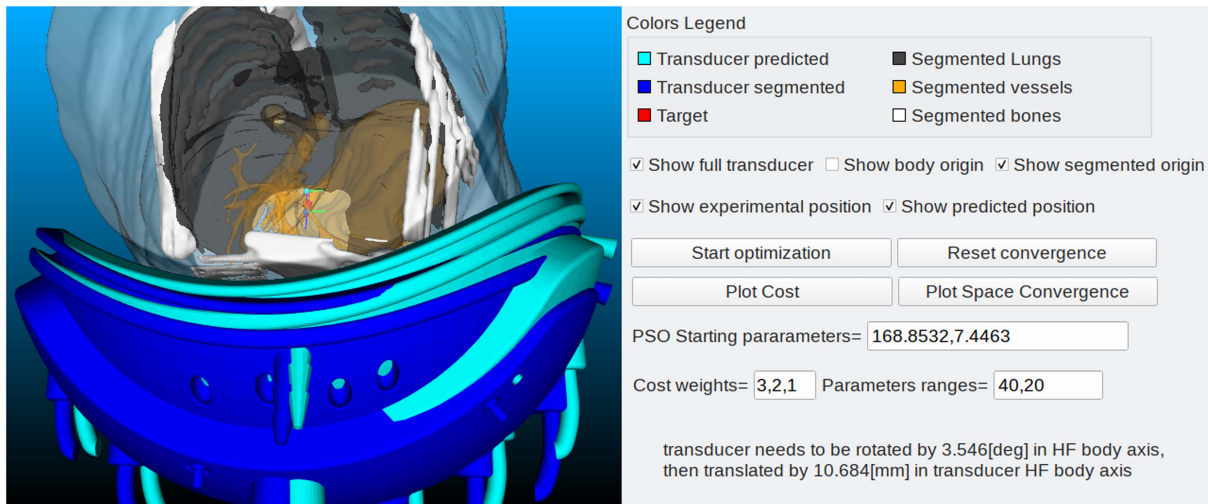
Fig. 5. Graphical user interface of the software showing the 3D reconstruction of the segmented body lying on the transducer and the functionalities of the software.

TABLE I
DIFFERENCES BETWEEN THE TOP AND THE EP USING TWO DoF

Pig	Differences between the TOP and the EP (° trigonometric, mm)	TOP vs EP ratio of the bone component of the cost function	Difference between the costs of the TOP and the EP, normalized to the maximum cost in the search space
1	10.2°/-7.3 mm	0.97	0.06
2	-12.0°/-7.0mm	0.79	0.11
3	-0.2°/-15.8mm	0.97	0.08
4	-4.4°/-8.0mm	0.88	0.09
5	-9.1°/2.8mm	0.83	0.04

iterative and manual process for the transducer positioning are in the Supplementary Material. The software computed the cost functions of the theoretical and the experimental positions and displayed the two positions in the graphical user interface (GUI) (Fig. 5). It also indicated the difference of the TOP compared to the EP using two DoF: along the depth axis of the transducer (abbreviated as "dist"), meaning a compression or a distance to the skin, and a rotation around the anatomic cranio-caudal direction (angle denoted as α). For evaluation purpose, an exhaustive heatmap of the cost function for the TOP was computed every 1 mm of depth and every 1° of rotation for each of the 5 pigs. The minimum TOP and EP cost functions were calculated and compared in Table I. The difference between the TOP and the EP was assessed by comparing the convergence point on the heatmaps. The robustness and consistency of the software was evaluated by repeating 50 times the PSO algorithm on each of the 5 pigs to conclude on the precision.

To explore the potential of the method, another DoF, namely a rotation around the long eigen axis of the transducer (angle denoted as β), was added and compared to the TOP given by 2 DoF. Adding a DoF is theoretical and could not be validated by the ground truth experimental data acquired with 2 DoF.

III. RESULTS

During the validation process conducted on five pigs, the mapping of the cost function with two DoF, across 80 rotations and 40 distances took a constant time of 115s and the computing time for the TOP using the PSO algorithm lasted 20s. This result is promising for real-time application intra-operatory.

The cost mapping, as illustrated in Fig. 4, revealed a monomodal form of the graph for the weight combination (1/2, 1/3, 1/6) leading to a unique optimal position or nearly optimal position. While these convergence points are not identical, their close proximity to each other — evidenced by a standard deviation of 1.5 degrees and 0.4 mm, and a maximum spread of 5.5 degrees and 2.2 mm — indicates a high degree of similarity in position. This reflects the robustness of the algorithm in consistently identifying near-optimal solutions within the defined search space.

Compared to the EP, the TOP optimized the rib cage and the software computed the mismatch of the TOP compared to the EP. The differences in the 5 pigs are presented in Table I.

The theoretical approach angles were similar to the experimental ones; however, the transducer during experiments was more distant to the skin compared to the computed one. The rotation difference was on average $-3.1 \pm 7.1°$ (-12.0 to $10.2°$) and the distance difference was on average -7.1 ± 5.4 mm (-15.8 to 2.8 mm).

When considering only physically possible solutions, the cost function for the bones is the most relevant parameter to analyze. Table I indicated that the cost function for the TOP was always lower than for the EP.

As demonstrated in Fig. 6(c) the consistent convergence of the algorithm to a similar region after 50 repetitions, even when initiated from significantly different starting points, underscores
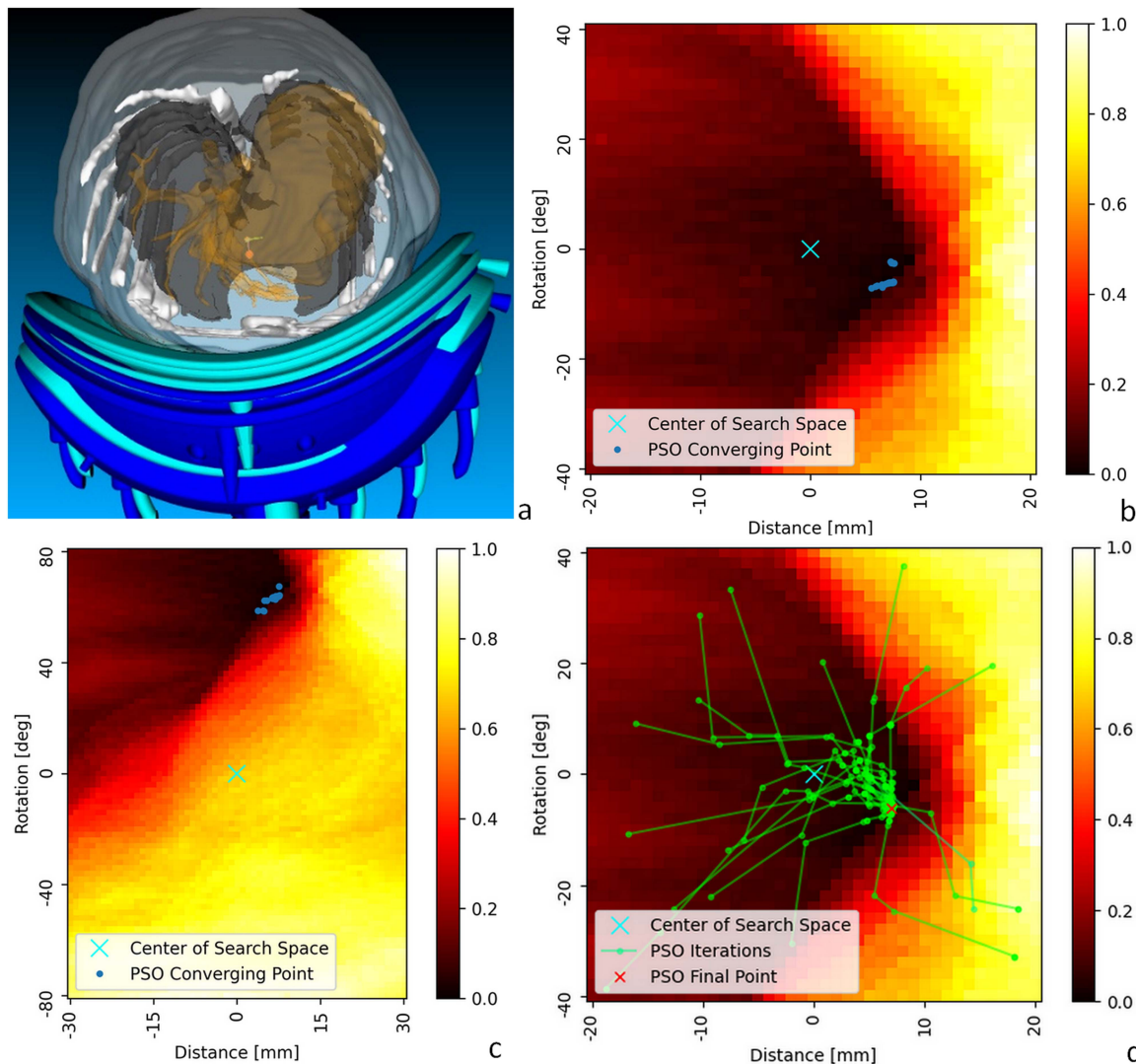
Fig. 6. (a) Displayed result after minimizing the cost function. The 3D representation of the segmented body lying on the CAD drawing of the transducer in the EOP (deep blue) is superimposed with the TOP (light blue). (b) Illustration of algorithm's precision overlapped on the exhaustive heatmapping of the cost function for Pig 4: note the final best positions obtained from 50 repeated runs of the PSO algorithm to evaluate the algorithm's consistency and precision. (c) Robustness of convergence: This panel illustrates the results of 50 repeated runs of the PSO algorithm, within an expanded search space deliberately centered far from the optimal position. (d) Single PSO run analysis: This figure presents the best solutions for individual particles as well as the overall best solution found in a single PSO run.

the robustness of our method and reliability of our approach in various scenarios.

Theoretically adding a DoF did not significantly impact the cost function and minimally impacted the TOP while keeping the computation time constant.

IV. DISCUSSION

The design of our super-convergent transducer [11], [28], spreading the incident energy over a large aperture and minimizing the secondary acoustic lobes, is the first key of its safe performance. As an additional layer, we describe the current optimization software. It was designed user-friendly with real-time and interactive visualization of the 3D segmentations and the CAD drawing of the transducer. The iterative process for the position calculation was fast, with a computing duration

not exceeding 20s, and could be significantly speed-up with parallel computing, which is compatible with intra-operatory execution. Nevertheless, the manual segmentation time of around 40 minutes should be considered in the total procedure time. The use of the software could drastically reduce the procedure duration for an MRgHIFU ablation, because an iterative and manual positioning necessitates 1-2h per session. Future improvements will focus on developing tools to automate this segmentation process, further reducing the time required for optimal transducer placement and enabling its prospective use intra-operatory.

For the establishment of heatmaps, the range for the distance to the target was set to ±20 mm to stay within the steering capacities of the transducer. Wherever the TOP is in the authorized range, the focal point should be electronically adjusted to shoot the target, and during positioning, the volume under the

membrane needs to be tuned up to compensate for the transducer moving closer or further away, without losing acoustic coupling.

A tumor that is too superficial or too profound is intrinsically inaccessible with this transducer anyway. The target should be located at least 2cm depth into the liver, which corresponds approximately to 4 cm from the skin in an average population.

The differences between the TOP and EP, using the data from the prior in vivo study and implementing two DoF, were comparable to the precision of convergence of the PSO (data not shown). The similarity between the TOP and the EP is a strong argument of the algorithm's efficacy, robustness and reliability. Lower cost functions in TOP even suggest that the EP could have been slightly optimized. The exhaustive heatmap, which represents the dense mapping of the cost function, was primarily included in the article for illustrative and validation purposes. This visualization provides insights into how each component of the cost function influences the overall calculation.

The mapping of the cost function was useful during the validation process to confirm the unique TOP, and analyze the evolution of the cost function with various weights, however the software does not intend to compute this mapping for daily use. The only output for the clinician is the coordinates of the TOP based on the PSO algorithm. Mapping the cost function with additional DoF in a higher dimension space would multiply the computation time by the number of samples in others dimensions.

The software demonstrated consistency and precision, supported by the suggestion of similar TOP when repeating the algorithm (Fig. 6(b)). The random generation of particles by the PSO algorithm may explain the small differences in the TOP. The probability of staying in a local minimum is drastically lowered by the attribution of high speed and inertia of each particle but may still occur. Repetition of the algorithm further helped avoiding this issue.

The program is modulable and easily adjustable to other constraints and tissue features. The starting point and initialization settings can be changed to fit other transducers, widening the indications and the targeted organs. For liver ablation, the software may also be used for the positioning of the reflective patch to avoid thermal effects, as described by Lorton et al. [11], [28]. The use may be extended to other purposes, such as proposing a personalized virtual planning before the intervention to assess the feasibility or the compliance with inclusion criteria. The software may be able to calculate an eligibility score based on anatomical criteria to help the clinician in the inclusion process. It could be applied to other applications including intraluminal [34] and transperineal targeting [35].

The EP distance to the skin mostly exceeded the retrospectively TOP calculated one. This could be explained by the experimental learning curve. The closer the transducer to the skin, the lower the risk of inducing thermal effects on the ribs, but the realization of the physical setup becomes more difficult. The distance is a trade-off between the rib thermal effects and the need for a cooling layer.

While the cost function may show slight improvements with additional iterations, the corresponding changes in rotation and translation are so minute that they are practically irrelevant,

TABLE II
INFLUENCE OF ADDING A DoF ON THE OPTIMAL POSITION, THE COST FUNCTION, AND THE COMPUTING TIME

Pig number	DoF	α	β	Dist [mm]	Cost	Time [s]
Pig 06	2	164.1	0.0	19.0	1.52	60
Pig 06	3	168.0	4.8	13.1	1.44	60
Pig 07	2	140.9	4.7	-5.7	2.2	60
Pig 07	3	141.3	3.7	-5.7	2.26	59
Pig 08	2	165.1	0.0	5.1	1.65	76
Pig 08	3	164.7	5.0	-3.7	1.44	75
Pig 09	2	169.0	0.0	7.5	1.22	71
Pig 09	3	169.0	1.6	9.6	1.17	60
Pig 10	2	158.6	0.0	-15.0	1.44	60
Pig 10	3	163.8	4.5	-14.0	1.25	60

that is, the numerical precision of the algorithm exceeds the physical accuracy achievable for the transducer positioning in a therapeutic scenario.

We made the approximation that the transducer was symmetrically aligned with the axial anatomical plane as our setup was designed to fit the pig morphology and the transducer orientation. We estimate the residual rotation less than 2°, which will be even lower in patients using a mechanized holder.

This study lacks data on the potential clinical improvement between the EP versus the TOP positioning, for instance in term of the thermal heating ratio at the target versus the ribs. This is a retrospective analysis from *in vivo* data, meaning that further evaluation in a prospective *in vivo* study is required to fully validate the approach. Furthermore, this paper does not report any simulation of the acoustic field and thermal profile, such as shadowing, rib heating, or acoustic interferences. Nonetheless, we used effective experimental data in vivo to confirm the relevance of the PSO algorithm. On the top of our element-wise ray tracing approach, cross-sectional calculations could be implemented by discretizing the acoustic hexagonal elements of the transducer. This will however linearly scale up with the computing time.

Another improvement would be the addition of more DoF for the transducer positioning. This study validated the algorithm considering rotation around the cranio-caudal axis (Ox in Fig. 1(b)) and the distance to the skin, while rotations around the Oy and Oz axes, or translation along the cranio-caudal direction (Ox) could further be included. The DoF were restricted to those with the greatest influence on the solution, since the focal point position can be anisotropically corrected in a volume of $\pm$ 14 mm, $\pm$ 23 mm and $\pm$ 25 mm by electronic beam forming along the short axis (Ox), the long axis (Oy) and the depth axis (Oz) of our transducer respectively. In addition, our experimental setup only afforded the two mentioned DoF. For multiple DoF the transducer holder needs to be modified. However, theoretically adding a rotation around Oy would minimally impact the suggested position as presented in Table II, but this was not validated by this retrospective study.

Furthermore, the precision of the positioning could be improved by computing a more elaborated cost function with additional terms in (1) that would be assigned with lower weights. Here, the PSO algorithm was validated by comparison with expert experimental positions that avoided air-filled structures such as empty stomach, lungs or bowels, not considered in (1). The structure of the cost function could be refined in future studies to cover the strong acoustic impedance discontinuities, subject to beam reflection and localized heating. For instance, the distance to lung or stomach, or an angulation to avoid focusing through a major blood vessel, could be considered.

The computation time of the PSO algorithm in humans should be in the same order of magnitude as the pig, provided the similar anatomy. However, the search space could be wider in humans depending on the patient size, as more particles may be required for a same ratio number of particles / numbers of possible positions.

V. Conclusion

The developed software tool is suggested to significantly support the optimization of transducer placement for abdominal HIFU treatments. By automating a previously manual and time-consuming process, it has the potential to significantly reduce treatment time and increase patient comfort while maximizing the ratio of energy deposited versus energy emitted. The suggested software is modulable, and the research of the optimal position is consistent. Future improvements would be focused on further automating the process of segmentation to provide better care for patients.

Supplementary Materials

In Supplementary Materials, we detail the materials and methods section, including the design of the transducer, the steps completed by the software, the parameters of the MR sequence and the process for the manual positioning of the transducer.

Conflict of Interest

The authors declare no conflict of interest.

Authors' Contributions

YM, CC, MEO, RS and OL contributed to the methodology. YM, CC and MEO were in charge of the software development. YM, PCG, AR, SB, RS and OL conducted the experiments and performed data analysis, CC, LAC, SB, PAP, TK, RS and OL validated and supervised the study. All authors contributed to the writing and revision of the manuscript, and approved the final version.

Acknowledgment

References

[1] B. D. de Senneville, C. Mougenot, B. Quesson, I. Dragonu, N. Grenier, and C. T. Moonen, "MR thermometry for monitoring tumor ablation," *Eur. Radiol.*, vol. 17, no. 9, pp. 2401–2410, Sep. 2007, doi: 10.1007/s00330-007-0646-6.

[2] K. Kuroda, "MR techniques for guiding high-intensity focused ultrasound (HIFU) treatments," *J. Magn. Reson. Imag.*, vol. 47, no. 2, pp. 316–331, Feb. 2018, doi: 10.1002/jmri.25770.

[3] N. McDannold, "Quantitative MRI-based temperature mapping based on the proton resonant frequency shift: Review of validation studies," *Int. J. Hyperthermia*, vol. 21, no. 6, pp. 533–546, Sep. 2005, doi: 10.1080/02656730500096073.

[4] Y. Ishihara et al., "A precise and fast temperature mapping using water proton chemical shift," *Magn. Reson. Med.*, vol. 34, no. 6, pp. 814–823, Dec. 1995, doi: 10.1002/mrm.1910340606.

[5] P. S. Steeg, "Targeting metastasis," *Nat. Rev. Cancer*, vol. 16, no. 4, pp. 201–218, Apr. 2016, doi: 10.1038/nrc.2016.25.

[6] K. Ganesh and J. Massague, "Targeting metastatic cancer," *Nature Med.*, vol. 27, no. 1, pp. 34–44, Jan. 2021, doi: 10.1038/s41591-020-01195-4.

[7] F. C. Chow and K. S. Chok, "Colorectal liver metastases: An update on multidisciplinary approach," *World J. Hepatol.*, vol. 11, no. 2, pp. 150–172, Feb. 2019, doi: 10.4254/wjh.v11.i2.150.

[8] E. K. Abdalla, R. Adam, A. J. Bilchik, D. Jaeck, J. N. Vauthey, and D. Mahvi, "Improving resectability of hepatic colorectal metastases: Expert consensus statement," *Ann. Surg. Oncol.*, vol. 13, no. 10, pp. 1271–1280, Oct. 2006, doi: 10.1245/s10434-006-9045-5.

[9] R. Stangl, A. Altendorf-Hofmann, R. M. Charnley, and J. Scheele, "Factors influencing the natural history of colorectal liver metastases," *Lancet*, vol. 343, no. 8910, pp. 1405–1410, Jun. 1994, doi: 10.1016/s0140-6736(94)92529-1.

[10] A. S. Sehmbi et al., "Systematic review of the role of high intensity focused ultrasound (HIFU) in treating malignant lesions of the hepatobiliary system," *HPB*, vol. 23, no. 2, pp. 187–196, Feb. 2021, doi: 10.1016/j.hpb.2020.06.013.

[11] O. Lorton et al., "In vivo thermal ablation of deep intrahepatic targets using a super-convergent MRgHIFU applicator and a pseudo-tumor model," *Cancers*, vol. 15, no. 15, Aug. 2023, doi: 10.3390/cancers15153961.

[12] B. Martin and J. H. McElhaney, "The acoustic properties of human skull bone," *J. Biomed. Mater. Res.*, vol. 5, no. 4, pp. 325–333, Jul. 1971, doi: 10.1002/jbm.820050405.

[13] G. Pinton, J. F. Aubry, E. Bossy, M. Muller, M. Pernot, and M. Tanter, "Attenuation, scattering, and absorption of ultrasound in the skull bone," *Med. Phys.*, vol. 39, no. 1, pp. 299–307, Jan. 2012, doi: 10.1118/1.3668316.

[14] NCRP, "Biological effects of ultrasound: Mechanisms and clinical implications," Nat. Council Radiat. Protection, Tech. Rep. 74, 1983.

[15] Z. Celicanin et al., "Hybrid ultrasound-MR guided HIFU treatment method with 3D motion compensation," *Magn. Reson. Med.*, vol. 79, no. 5, pp. 2511–2523, May 2018, doi: 10.1002/mrm.26897.

[16] O. Lorton et al., "Self-scanned HIFU ablation of moving tissue using real-time hybrid US-MR imaging," *IEEE Trans. Biomed. Eng.*, vol. 66, no. 8, pp. 2182–2191, Aug. 2019, doi: 10.1109/TBME.2018.2885233.

[17] V. Auboiroux, L. Petrusca, M. Viallon, T. Goget, C. D. Becker, and R. Salomir, "Ultrasonography-based 2D motion-compensated HIFU sonication integrated with reference-free MR temperature monitoring: A feasibility study ex vivo," *Phys. Med. Biol.*, vol. 57, no. 10, pp. N159–N171, May 2012, doi: 10.1088/0031-9155/57/10/N159.

[18] Z. Celicanin et al., "Real-time method for motion-compensated MR thermometry and MRgHIFU treatment in abdominal organs," *Magn. Reson. Med.*, vol. 72, no. 4, pp. 1087–1095, Oct. 2014, doi: 10.1002/mrm.25017.

[19] M. Anzidei et al., "Magnetic resonance-guided focused ultrasound ablation in abdominal moving organs: A feasibility study in selected cases of pancreatic and liver cancer," *Cardiovasc. Intervent. Radiol.*, vol. 37, no. 6, pp. 1611–1617, Dec. 2014, doi: 10.1007/s00270-014-0861-x.

[20] F. Wu et al., "Extracorporeal high intensity focused ultrasound ablation in the treatment of patients with large hepatocellular carcinoma," *Ann. Surg. Oncol.*, vol. 11, no. 12, pp. 1061–1069, Dec. 2004, doi: 10.1245/ASO.2004.02.026.

[21] H. Zhu et al., "High intensity focused ultrasound (HIFU) therapy for local treatment of hepatocellular carcinoma: Role of partial rib resection," *Eur. J. Radiol.*, vol. 72, no. 1, pp. 160–166, Oct. 2009, doi: 10.1016/j.ejrad.2008.07.003.

[22] B. Quesson et al., "A method for MRI guidance of intercostal high intensity focused ultrasound ablation in the liver," *Med. Phys.*, vol. 37, no. 6, pp. 2533–2540, Jun. 2010, doi: 10.1118/1.3413996.

[23] M. Zubair and R. Dickinson, "Calculating the effect of ribs on the focus quality of a therapeutic spherical random phased array," *Sensors*, vol. 21, no. 4, Feb. 2021, doi: 10.3390/s21041211.

[24] D. McMahon and M. Almekkawy, "Elements selection for transcostal HIFU refocusing method: Simulation study," *IEEE Trans. Ultrason. Ferroelect. Freq. Control*, vol. 67, no. 7, pp. 1366–1376, Jul. 2020, doi: 10.1109/TUFFC.2020.2973678.

[25] R. Salomir et al., "Magnetic resonance-guided shielding of prefocal acoustic obstacles in focused ultrasound therapy: Application to intercostal ablation in liver," *Invest. Radiol.*, vol. 48, no. 6, pp. 366–380, Jun. 2013, doi: 10.1097/RLI.0b013e31827a90d7.

[26] P. Ramaekers, M. Ries, C. T. Moonen, and M. de Greef, "Improved intercostal HIFU ablation using a phased array transducer based on Fermat's spiral and Voronoi tessellation: A numerical evaluation," *Med. Phys.*, vol. 44, no. 3, pp. 1071–1088, Mar. 2017, doi: 10.1002/mp.12082.

[27] V. Auboiroux, E. Dumont, L. Petrusca, M. Viallon, and R. Salomir, "An MR-compliant phased-array HIFU transducer with augmented steering range, dedicated to abdominal thermotherapy," *Phys. Med. Biol.*, vol. 56, no. 12, pp. 3563–3582, Jun. 2011, doi: 10.1088/0031-9155/56/12/008.

[28] O. Lorton et al., "A novel concept of a phased-array HIFU transducer optimized for MR-guided hepatic ablation: Embodiment and first In-vivo studies," *Front. Oncol.*, vol. 12, 2022, Art. no. 899440, doi: 10.3389/fonc.2022.899440.

[29] T. Y. Park, K. J. Pahk, and H. Kim, "Method to optimize the placement of a single-element transducer for transcranial focused ultrasound," *Comput. Methods Programs Biomed.*, vol. 179, Oct. 2019, Art. no. 104982, doi: 10.1016/j.cmpb.2019.104982.

[30] M. V. Joseph Blackmore, C. Butler, and R. Cleveland, "Focusing ultrasound through the skull for neuromodulation," *J. Acoust. Soc. Amer.*, vol. 141, no. 5_Suppl., 2017.

[31] T. Y. Park, H. J. Kim, S. H. Park, W. S. Chang, H. Kim, and K. Yoon, "Differential evolution method to find optimal location of a single-element transducer for transcranial focused ultrasound therapy," *Comput. Methods Programs Biomed.*, vol. 219, Jun. 2022, Art. no. 106777, doi: 10.1016/j.cmpb.2022.106777.

[32] J. Kennedy and R. Eberhart, "Particle swarm optimization," in *Proc. Int. Conf. Neural Netw.*, 1995, pp. 1942–4948, doi: 10.1109/ICNN.1995.488968.

[33] A. Fedorov et al., "3D Slicer as an image computing platform for the Quantitative Imaging Network," *Magn. Reson. Imag.*, vol. 30, no. 9, pp. 1323–1341, Nov. 2012, doi: 10.1016/j.mri.2012.05.001.

[34] D. Melodelima et al., "Intraluminal ultrasound applicator compatible with magnetic resonance imaging 'real-time' temperature mapping for the treatment of oesophageal tumours: An ex vivo study," *Med. Phys.*, vol. 31, no. 2, pp. 236–244, Feb. 2004, doi: 10.1118/1.1634909.

[35] P. C. Guillemin et al., "A novel concept of transperineal focused ultrasound transducer for prostate cancer local deep hyperthermia treatments," *Cancers*, vol. 15, no. 1, Dec. 2022, Art. no. 163, doi: 10.3390/cancers15010163.